SAND2021-5726C

Shoulder fillet effects in strength distributions of polysilicon MEMS

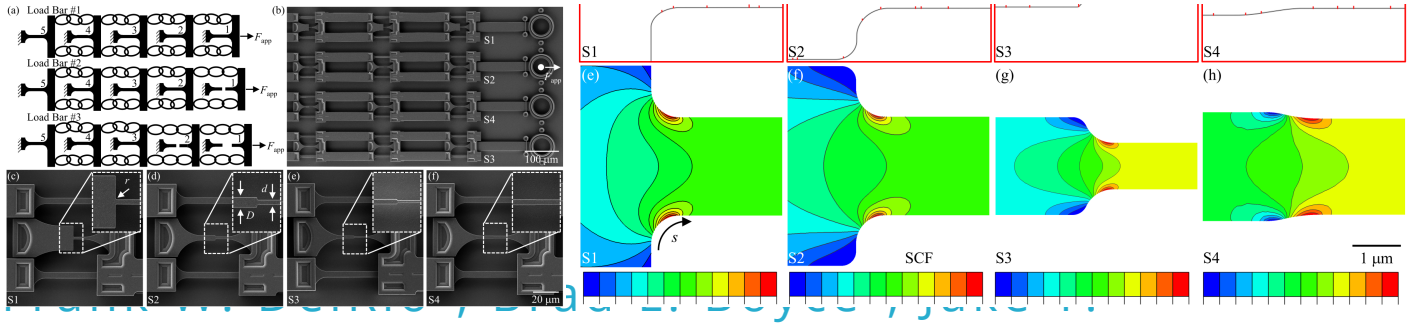

Frank W. Delrio[1], Brad L. Boyce[1], Jake A. Benzing[2], Lawrence H. Friedman[3], and Robert F. Cook[3]

[1]Material, Physical, and Chemical Sciences Center, Sandia National Laboratories, Albuquerque, NM 87185, USA
[2]Material Measurement Laboratory, National Institute of Standards and Technology, Boulder, CO 80305, USA
[3]Material Measurement Laboratory, National Institute of Standards and Technology, Gaithersburg, MD 20899, USA

Sandia National Laboratories is a multimission laboratory managed and operated by National Technology & Engineering Solutions of Sandia, LLC, a wholly owned subsidiary of Honeywell International Inc., for the U.S. Department of Energy's National Nuclear Security Administration under contract DE-NA0003525.

Polysilicon micro- and nanoscale components: the problem

Silicon is the primary substrate and structural material used to create both microelectronics and MEMS devices. Processing methods have been thoroughly developed by the electronics industry and adapted for MEMS production.

Capabilities

Basic Actuators (2-level)

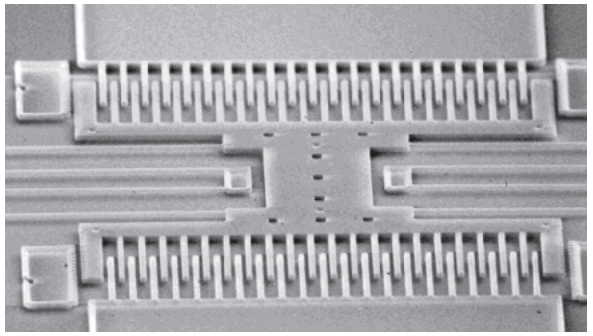

Gears and Hubs (3-level)

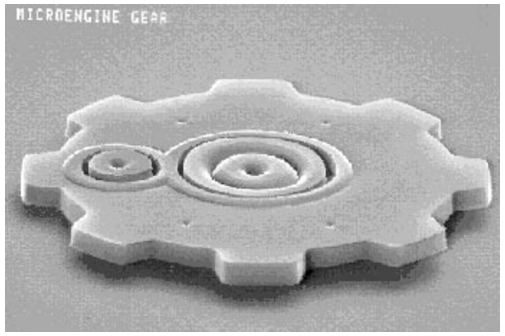

Linkage Elements (4-level)

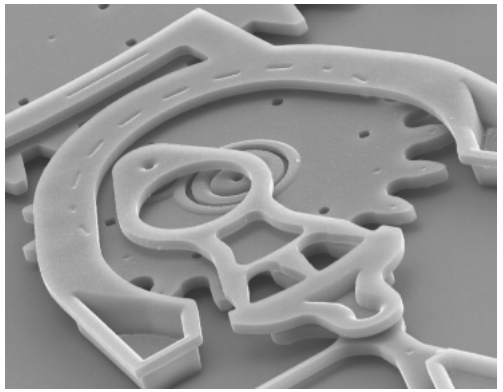

Complex Systems (5-level)

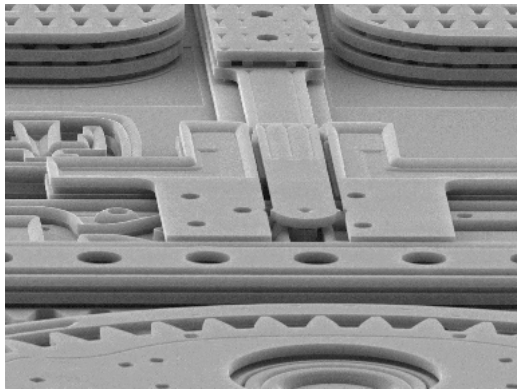

Sniegowski and de Boer, *Annu. Rev. Mater. Sci.* **30**, 299 (2000).

Reasons for Widespread Usage

- Multi-level components
- Low residual in-plane stress
- High degree of flatness
- High deposition rate
- Vertical sidewalls
- High etch selectivity (oxide)
- High degree of conformality
- High strength
- Low adhesion/friction
- CMOS compatible; well-established
- n- and p-type doping possible

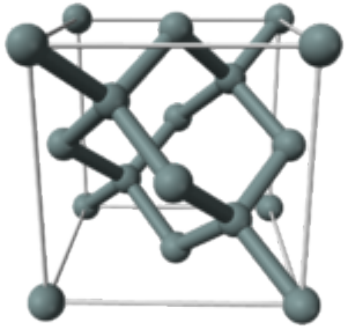

en.wikipedia.org/wiki/Silicon

Problem: Need experimental test methods and analytical frameworks to predict strength distributions for arbitrary MEMS structures from simple tensile testing geometries.

Polysilicon micro- and nanoscale components: a solution

Solution: The connection between strength measurements on simple tensile testing geometries and strength predictions on arbitrary MEMS structures is the accurate determination of the underlying flaw size distribution and spatial density.

High-throughput Fracture Testing

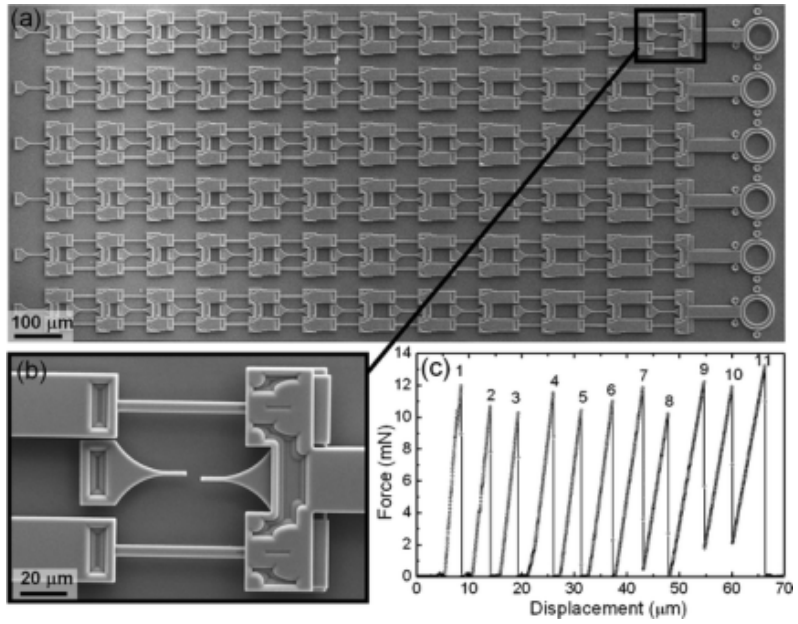

Boyce, *Exp. Mech.* **50**, 993 (2010).

Analytical Framework

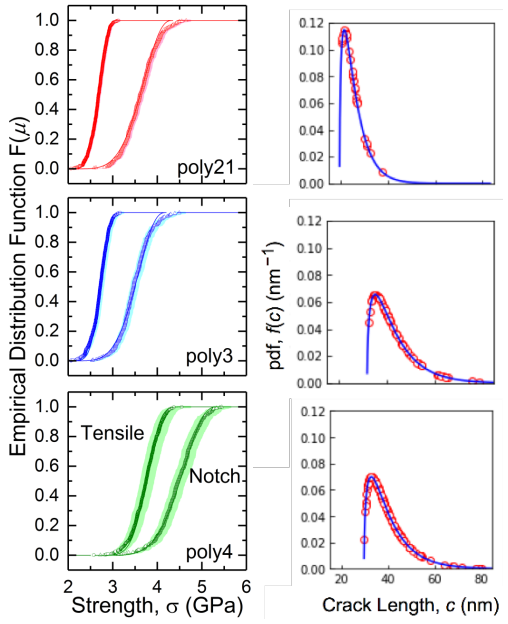

Cook *et al.*, *Microsys. Nanoeng.* **5**, 49 (2019).

Monte Carlo and FEA Simulations

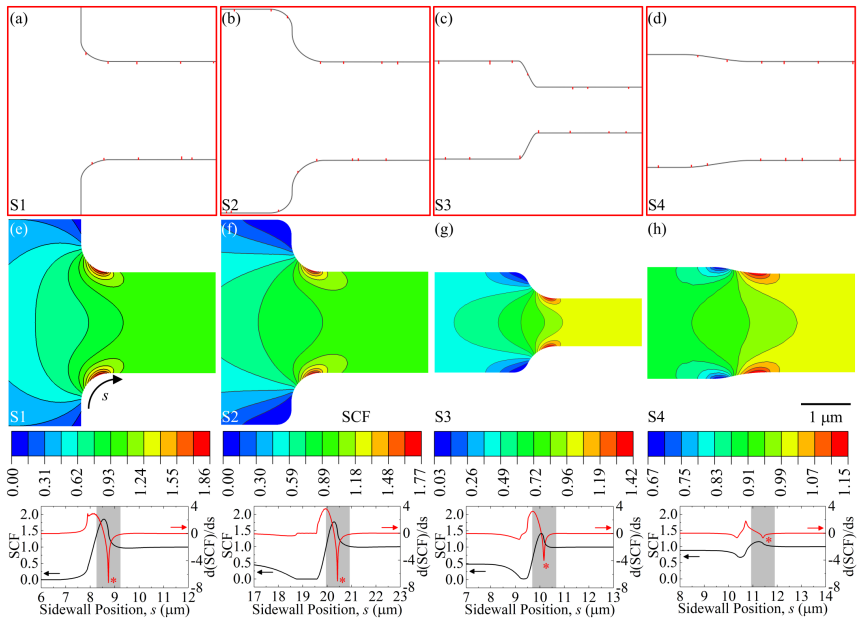

DelRio *et al.*, *J. Micromech. Microeng.* **30**, 125013 (2020).

Step 1: High-throughput test methods to assess strengths for tensile and fillet geometries.

Step 2: Analytical framework to translate strength distributions to flaw population.

Step 3: Monte Carlo and FEA to visualize flaws and stresses relative to specimen geometry.

High-throughput testing: method

Concept

- Force is applied at the end of first specimen.
- After fracture, slack is taken up in the chain.
- Repeat process for all specimens in the chain.
- Allows for a 1000 tests in 16 hr of testing.

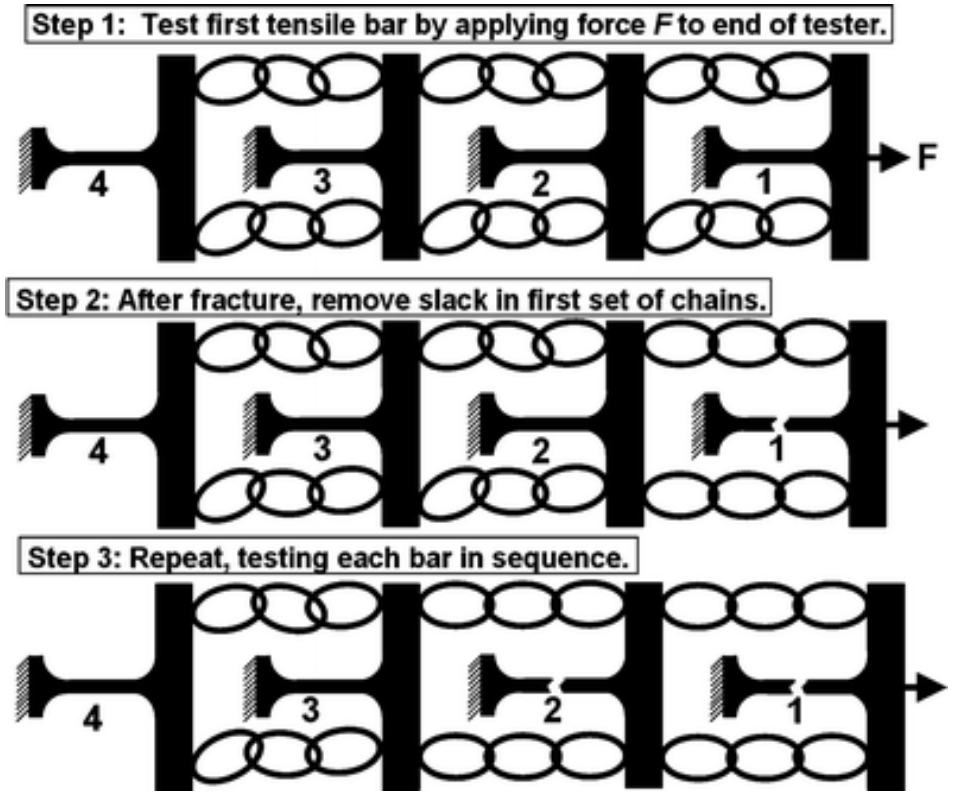

Boyce, *Exp. Mech.* **50**, 993 (2010).

Process

- Insert a FIB machined tungsten peg into a ring attached to the free end. Determine fracture force for each bar.
- Calculate the fracture strengths from the fracture forces and the specimen geometries measured from SEM.

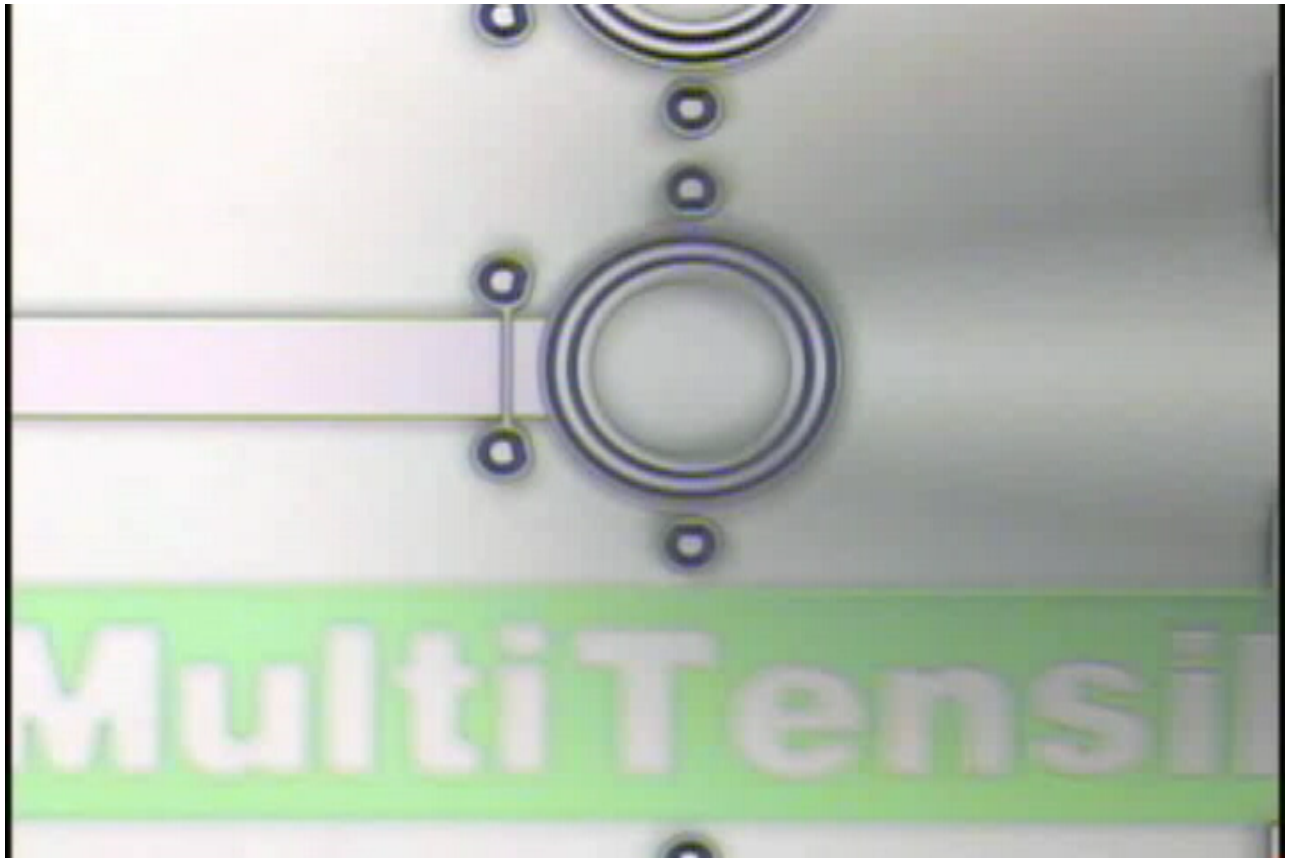

High-throughput testing: fabrication and geometries

Fabrication

- Devices fabricated from polysilicon in the SUMMiT V™ process.
- One layer was investigated: poly3 (thickness = 2.33 μm).
- All samples fabricated from a single reticle set (RS723).

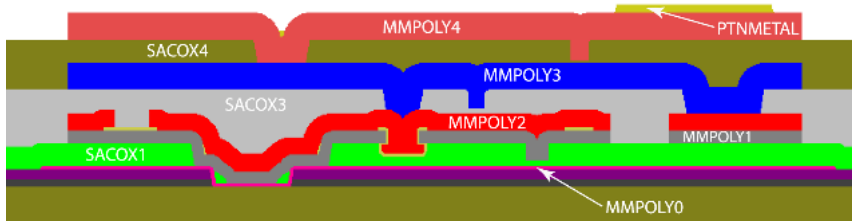

SUMMiT V™ Design Manual (www.sandia.gov)

Test Geometries

- Four different geometries (S1-S4) with different fillet geometries.
- Nominal widths (*D*, *d*) were S1 (20 μm, 2 μm), S2 (4 μm, 2 μm), S3 (2 μm, 1 μm), and S4 (2.25 μm, 2 μm). Designed with 90° angles at interface.
- Actual dimensions measured via SEM. *D* and *d* were less than nominal values. *r* were similar for S1 to S3 but increased for S4.
- 130-170 specimens per group.

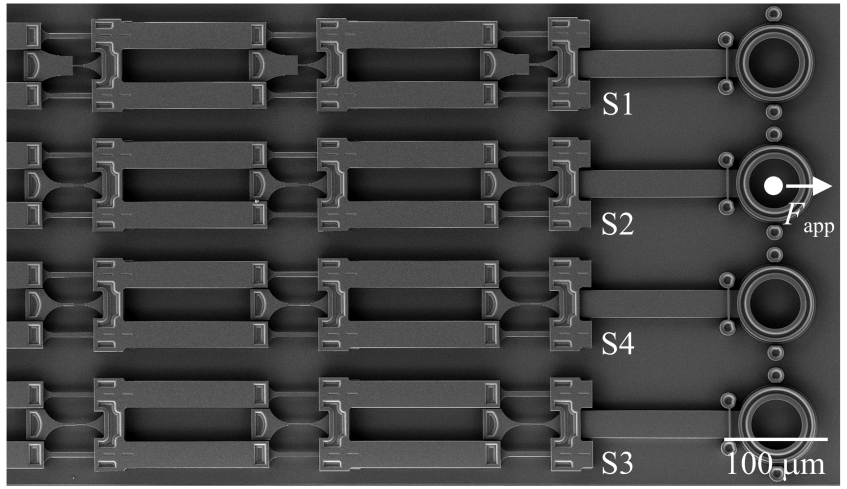

Type	Number of Specimens, *N*	Maximum Width, *D* (μm)	Minimum Width, *d* (μm)	Shoulder Radius, r (μm)
S1	133	19.32 ± 0.06	1.91 ± 0.02	0.54 ± 0.02
S2	162	3.85 ± 0.03	1.90 ± 0.03	0.55 ± 0.03
S3	170	1.89 ± 0.03	0.90 ± 0.02	0.58 ± 0.02
S4	153	2.14 ± 0.02	1.89 ± 0.02	3.04 ± 0.04

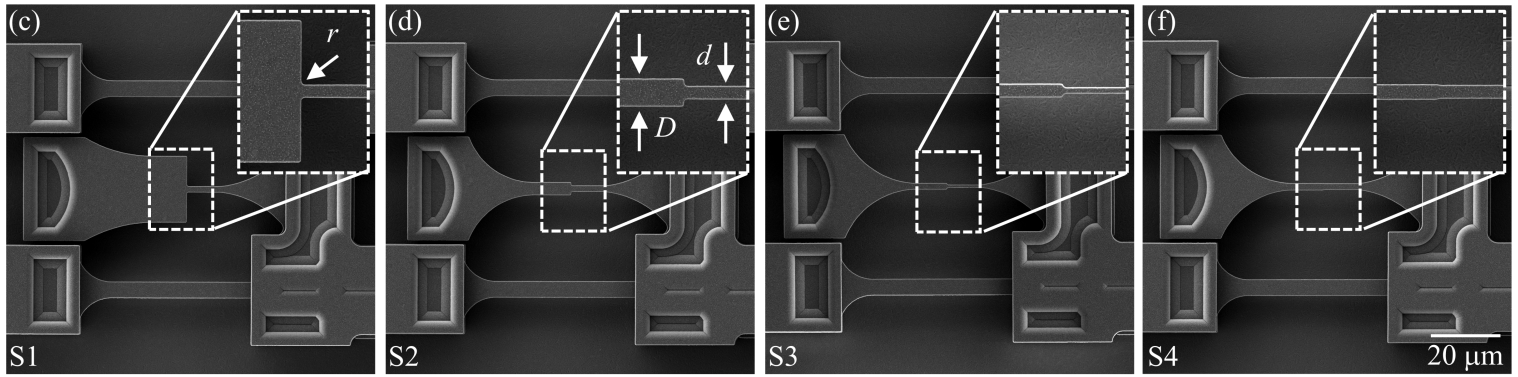

DelRio *et al.*, *J. Micromech. Microeng.* **30**, 125013 (2020).

High-throughput testing: calculations and locations

Strength Calculations

- Fracture force F_f taken just prior to fracture.
- Gauge section stress determined from $\sigma_g = F_f/(dh)$.
- Fracture strength calculated via $\sigma_f = K_t F_f/(dh)$.
- K_t is the stress concentration factor; decreased from S1 to S4.

Strength Results

- F_f distributions were sigmoidal in shape and distinguishable.
- σ_g decreased in the following specimen order: S4, S3, S2, and S1.
- σ_f curves for the S1 and S2 specimens were nearly identical, but then shifted to smaller σ_f values for the S3 and S4 specimens.

Fracture Locations

- S1 and S2 specimens failed solely in the shoulder fillet region.
- S3 and S4 failure region extended into the small gauge section.

Type	Analytical SCF, K_t	FEA SCF, K_t
S1	1.84	1.86
S2	1.72	1.77
S3	1.40	1.42
S4	1.15	1.15

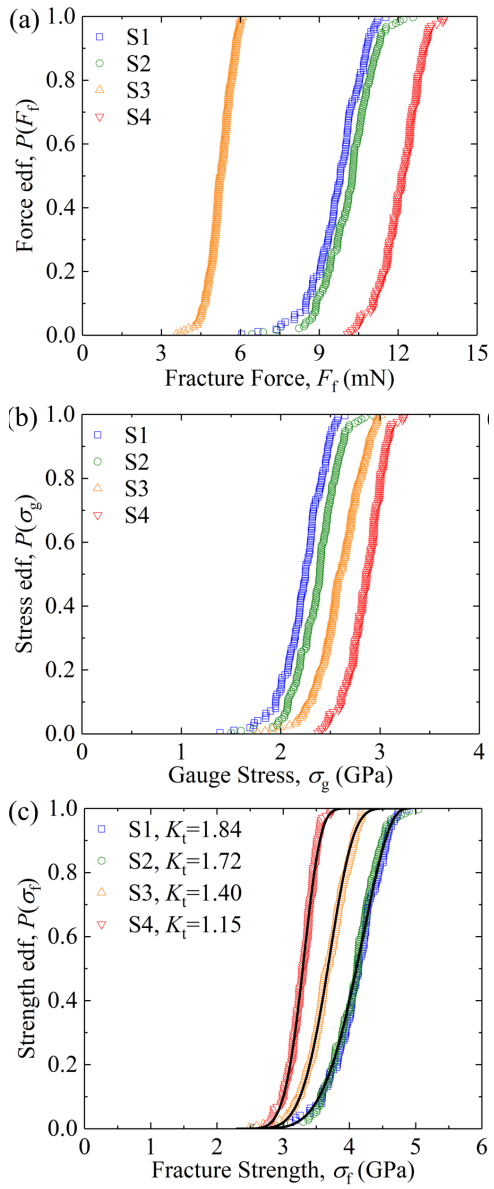

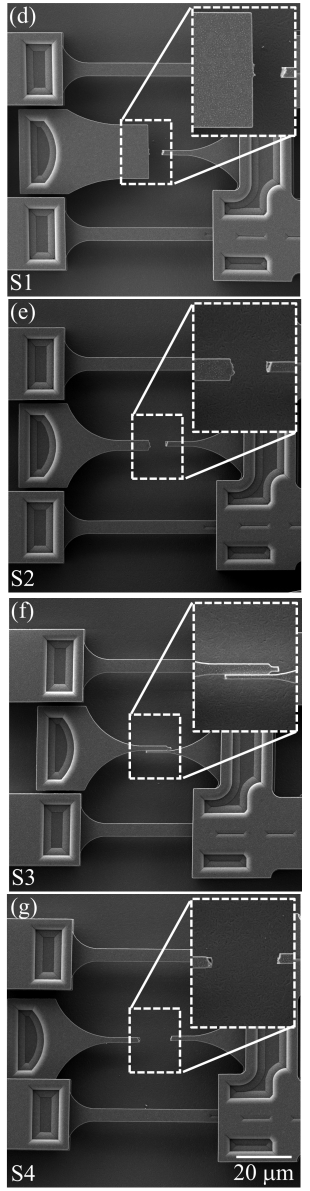

DelRio *et al.*, *J. Micromech. Microeng.* **30**, 125013 (2020).

Analytical framework: general procedure

Strength Distributions

Strength distribution of the S1 specimens was fit to a continuous sigmoidal function

$$F(\mu) = 30\left[(\mu^{3p}/3) - (\mu^{4p}/2) + (\mu^{5p}/5)\right] \quad \text{where} \quad \mu = (\sigma - \sigma_{th})/(\sigma_u - \sigma_{th})$$

Type	Lower bound, σ_{th} (GPa)	Upper bound, σ_u (GPa)	Exponent, p
S1	2.20	4.30	1.8

Flaw Size Distribution $f(c)$

- Consider S1 cdf (weakest-link)

$$F(c) = [1 - F(\mu)]^{\Delta L/L} = [1 - F(\mu)]^{1/2}$$

- Utilize Griffith equation

$$\sigma = Bc^{-1/2} \quad \text{where} \quad B = 0.75 \text{ MPa m}^{1/2}$$

- Determine flaw size pdf

$$f(c) = dF(c)/dc$$

Length Scaling Factor L_n/L_1

- Length over which flaws are active (relative to the S1 geometry).
- Consider S2, S3, S4 cdfs (weakest-link)

$$F(c) = [1 - F_1(\mu)]^{\Delta L/L_1} \quad F(c) = [1 - F_n(\mu)]^{\Delta L/L_n}$$

$$F_n(\mu) = 1 - [1 - F_1(\mu)]^{(L_n/L_1)}$$

- L_2/L_1, L_3/L_1, and L_4/L_1 are fitting parameters.

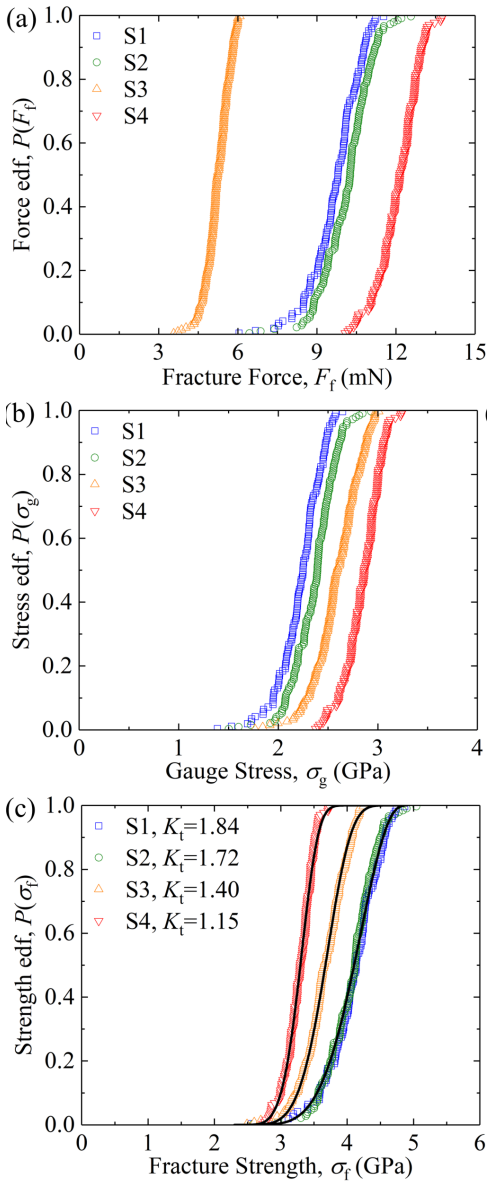

Cook and DelRio, *Exp. Mech.* **59**, 279 (2019). Cook and DelRio, *J. Amer. Ceram. Soc.* **102**, 4794 (2019). DelRio *et al.*, *J. Micromech. Microeng.* **30**, 125013 (2020).

Analytical framework: flaw size distribution

Flaw Size Distribution

- The flaw size pdf is asymmetric, consisting of many small flaws and an extended large flaw tail.
- The flaws are in ranges of 20 nm or 30 nm to approximately 70 nm, comparable to the dimensional dispersions.
- The domain of flaw sizes is nearly equivalent to results from another reticle set for the poly3 layer, demonstrating reticle-to-reticle reproducibility.

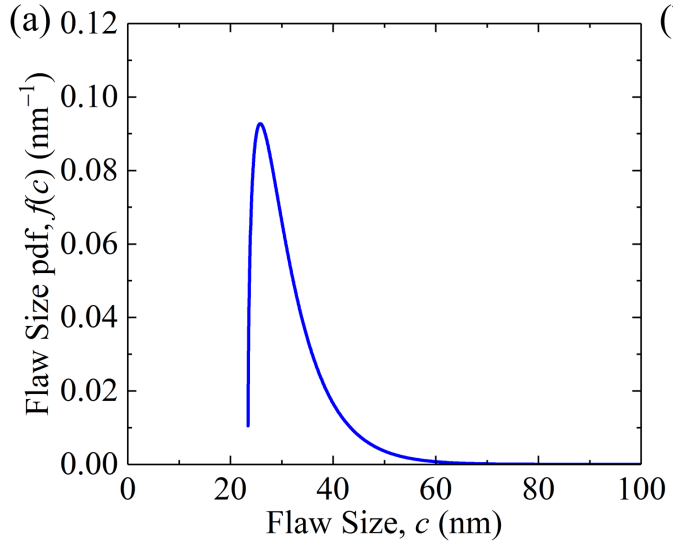

DelRio *et al.*, *J. Micromech. Microeng.* **30**, 125013 (2020).

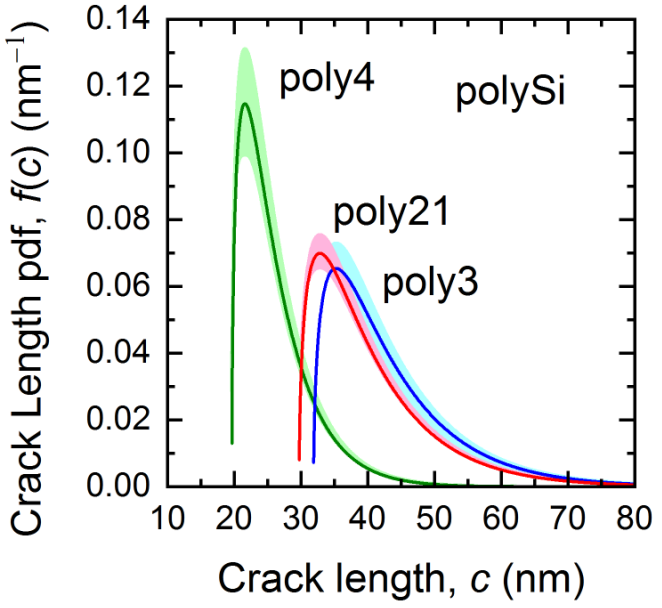

Cook *et al.*, *Microsys. Nanoeng.* **5**, 49 (2019).

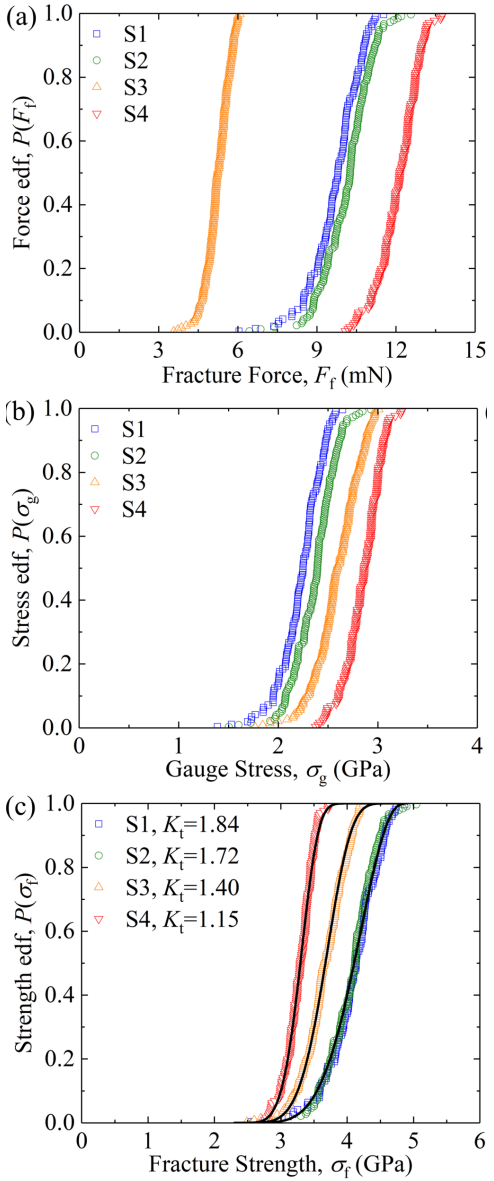

DelRio *et al.*, *J. Micromech. Microeng.* **30**, 125013 (2020).

Analytical framework: length scaling factor

Overall Trends

- Length scaling factor was initially constant and then increased as SCF decreased due to change in stress concentrating effects.

Type	Analytical SCF, K_t	Length Scaling Factor L_n/L_1
S1	1.84	–
S2	1.72	1
S3	1.40	4
S4	1.15	21

Distinct Regions

- In region 1, $L_2/L_1 = 1$, suggesting the SCF is large enough to ensure failure from a single flaw in the fillet region.
- In region 2, L_2/L_1 increases as the SCF decreases, suggesting that the length over which flaws are active increases.
- In region 3, the length scaling factor can decrease or increase with the length of the tensile bar.

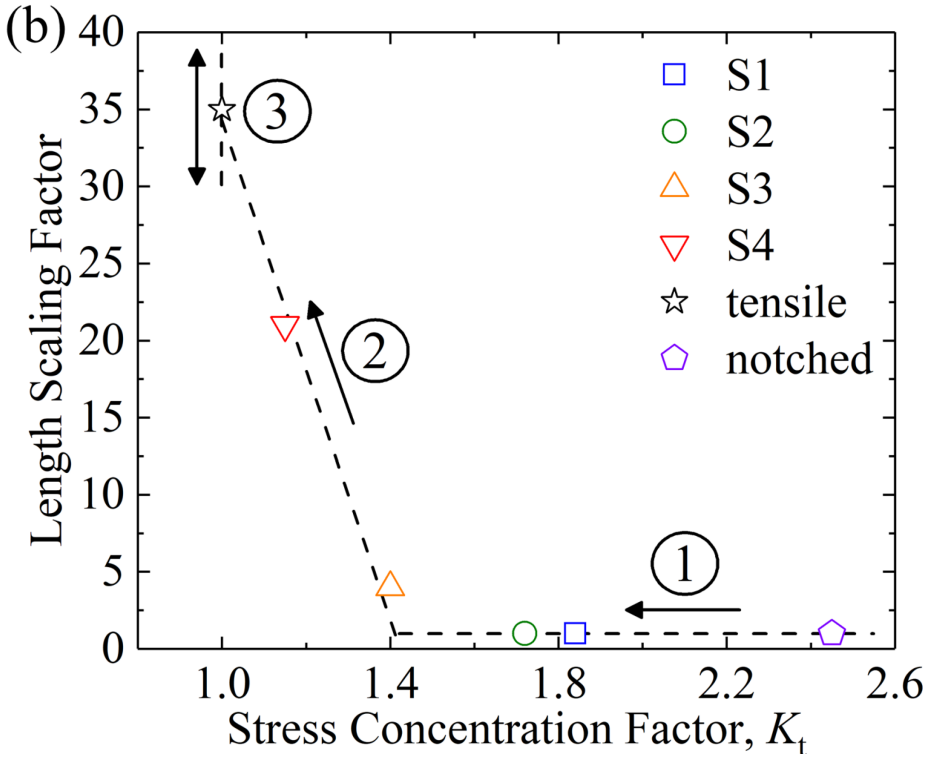

DelRio *et al.*, *J. Micromech. Microeng.* **30**, 125013 (2020).

Tensile (K_t = 1) and notched (K_t = 2.45) poly3 data are also shown for reference.

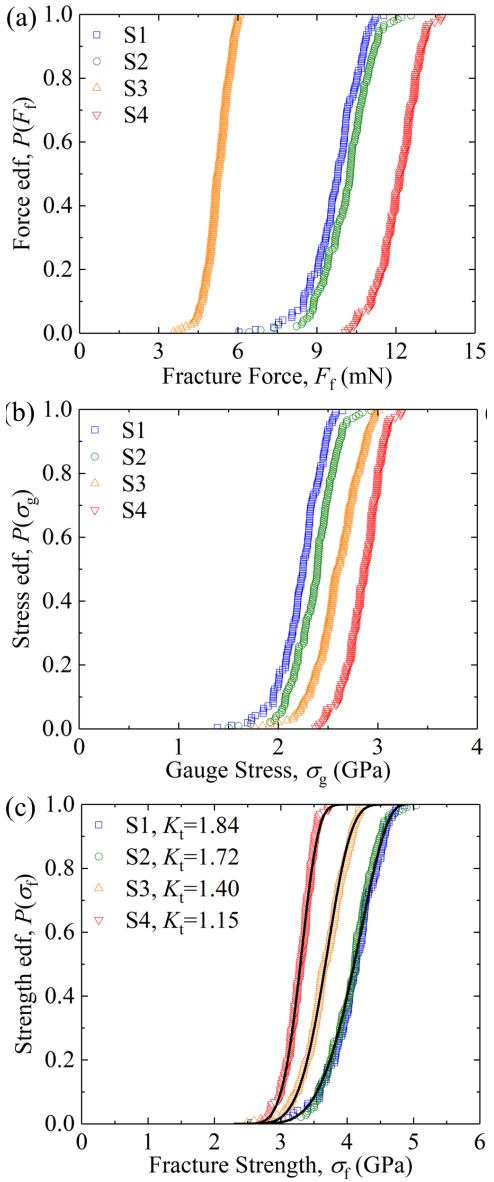

DelRio *et al.*, *J. Micromech. Microeng.* **30**, 125013 (2020).

Monte Carlo simulations

Monte Carlo Approach

- Facilitated a quantitative assessment of the *flaw size distribution and length scaling factors relative to specimen geometry.*
- The flaw sizes were selected randomly from $f(c)$ as assessed from S1 specimens.
- The flaw spacings were sampled from a uniform ΔL distribution with a mean of 0.57 μm and range of ±0.48 μm about the mean.

Monte Carlo Results

- For S2 specimens, $\Delta L \approx \pi R/2$ and $L_2/L_1=1$: single flaw in fillet, failure from flaw.
- For S3 specimens, $\Delta L \approx \pi R/2$ and $L_3/L_1>1$: single flaw in fillet, failure outside fillet.
- For S4 specimens, $\Delta L < \pi R/2$ and $L_4/L_1>1$: several flaws in fillet, failure outside fillet.

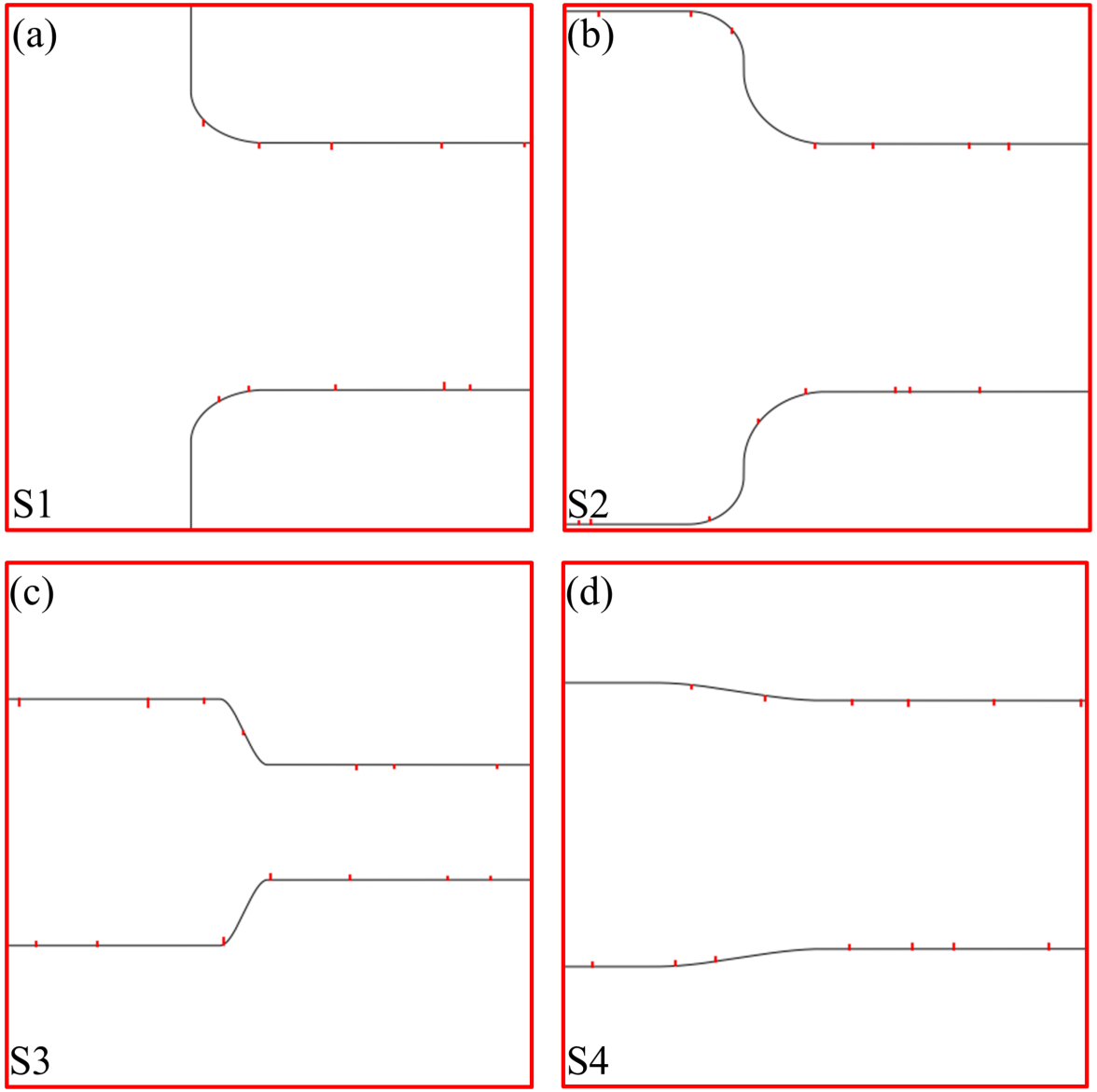

DelRio *et al.*, *J. Micromech. Microeng.* **30**, 125013 (2020).

Finite element analysis simulations

FEA Approach

- Facilitated a quantitative assessment of the *stress fields relative to specimen geometry.*
- Loaded axially with unit stress so maximum principal stress contours equaled SCFs.
- Linear plane-stress constitutive laws.
- Adaptive meshing of second-order triangles verified that models converged to 0.1%.

FEA Results

- Both SCFs (black lines) and derivatives of SCFs with *s* (red lines) were plotted.
- The width of the derivative peak was initially well contained for the S1 and S2 specimens and then spread for the S3 and S4 specimens.
- Fracture was localized for the S1 and S2 specimens but spread into the minimum width region for the S3 and S4 specimens.

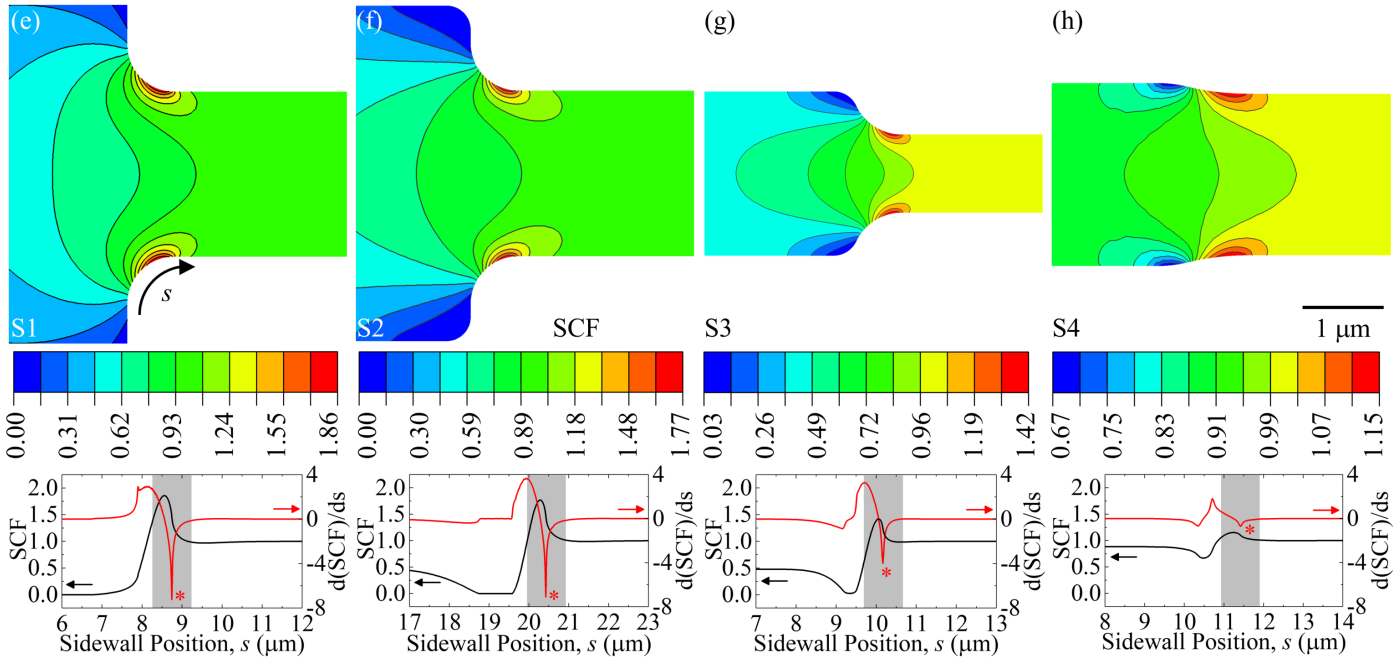

Type	Analytical SCF, K_t	FEA SCF, K_t
S1	1.84	1.86
S2	1.72	1.77
S3	1.40	1.42
S4	1.15	1.15

DelRio *et al.*, *J. Micromech. Microeng.* **30**, 125013 (2020).

SCFs from the FEA were in good agreement with those from the analytical solutions.

Conclusions and future work

Conclusions

- High-throughput testing via the slack-chain geometry provided statistically-significant descriptions of the strength distributions.
- Extension of the weakest-link-based framework to another geometry provides further empirical support for the mathematical structure.
- SCFs determined by an analytical method were verified by FEA, providing confidence in application of the analytical SCF expressions.

Future Work

- Different specimen geometries and loading modes
- Different strength-flaw size relationships (notch, cusp)
- Different materials (ductile vs. brittle)

Acknowledgements

- Center for Integrated Nanotechnologies

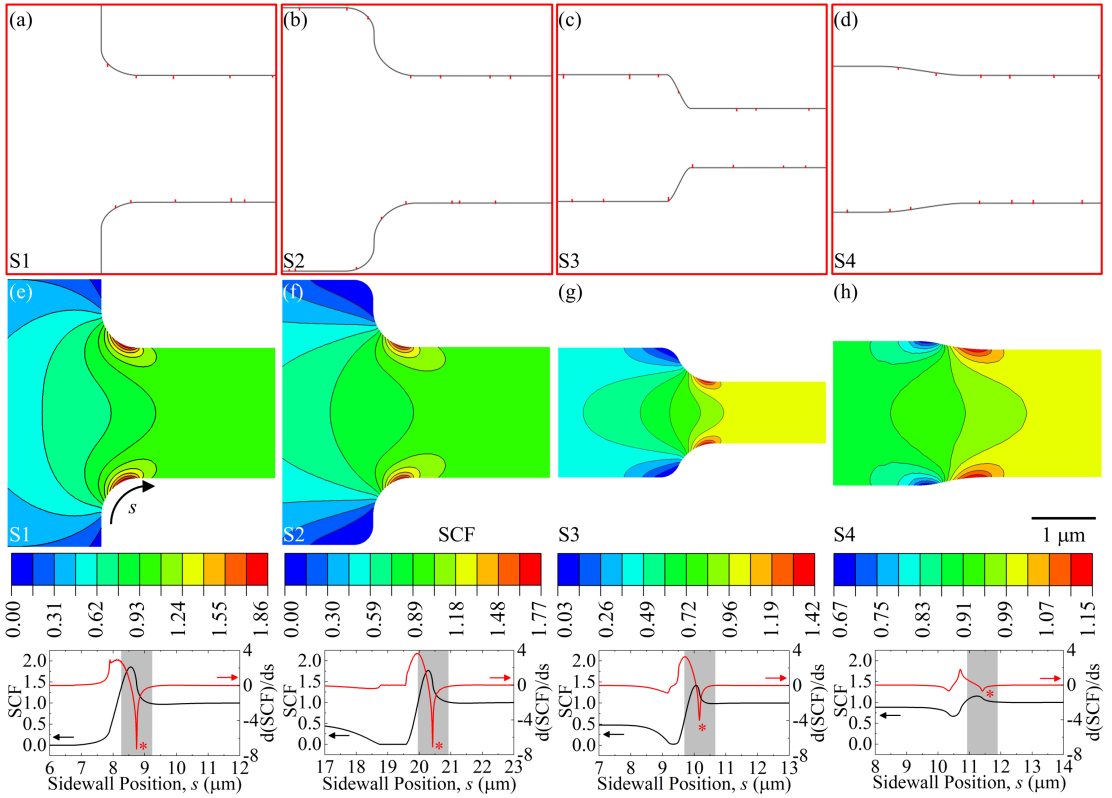

DelRio *et al.*, *J. Micromech. Microeng.* **30**, 125013 (2020).

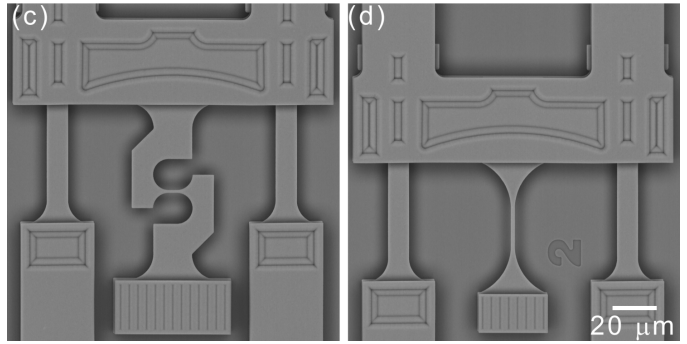

Cook *et al.*, *Appl. Phys. Lett.* (in press).